Magnetothermal behavior of a nanoscale Fe/Fe oxide granular system

L. Del Bianco*
Istituto Nazionale per la Fisica della Materia, Unità di Bologna, c/o Dipartimento di Fisica, Università di Bologna, Viale Berti Pichat 6/2, I-40127 Bologna, Italy

D. Fiorani and A. M. Testa
Istituto di Struttura della Materia—CNR, C.P. 10, 00016 Monterotondo Stazione (Roma), Italy

E. Bonetti and L. Savini
Dipartimento di Fisica, Università di Bologna and INFM, I-40127 Bologna, Italy

S. Signoretti
Swiss Federal Institute of Technology (ETH) Zurich, CH-8093 Zurich, Switzerland
(Received 12 April 2002; revised manuscript received 20 June 2002; published 11 November 2002)

The low-temperature magnetic properties of samples obtained by cold-compacting core-shell Fe/Fe oxide nanoparticles have been investigated, and their dependence on the structure, composition, and mean particle size D has been discussed. Samples with different D, varying from 6 to 15 nm, and different Fe to oxide ratio were analyzed by means of transmission electron microscopy, x-ray diffraction, and magnetization measurements in the 5–300-K temperature range. The results support the existence of a low-temperature (below $T_1 \sim 20$ K) frozen, disordered magnetic state, characterized by a strong exchange coupling between the structurally disordered, spin-glass-like oxide matrix and the Fe nanocrystallites. Above T_1, a different regime is distinguished, characterized by the coexistence of a quasi-static, ferromagnetic component, given by the Fe particles, and a relaxing component, represented by regions of exchange-interacting spins of the oxide matrix. As the temperature is increased above T_1, the net moments of the oxide magnetic regions become able to thermally fluctuate and they tend to be polarized by the Fe particle moments. The above picture well accounts for the composition, particle size, and thermal dependence of the coercivity and of the exchange field, which strongly increase with reducing temperature in correspondence with the freezing of most of the moments of the oxide magnetic regions.

DOI: 10.1103/PhysRevB.66.174418 PACS number(s): 75.50.Tt, 75.50.Lk, 75.50.Bb

I. INTRODUCTION

A common characteristic of nanostructured magnetic materials is the coexistence of two or more phases, magnetically and/or structurally different, which are modulated on a length scale of the order of a nanometer.[1–6] It was recently demonstrated that ultrafine ferrite particles can also be considered as heterogeneous systems. In fact, the surface region exhibits modified magnetic properties compared to the bulk as a consequence of the lack of structural periodicity and of the presence of competing magnetic interactions, resulting in spin canting and spin-glass-like behavior.[7–9] The coexistence of topological disorder and frustration of magnetic interactions has also been found to lead to similar phenomena in metallic systems.[10,11] A notable example is the observation of a spin-glass-like freezing at the grain boundary in ball-milled nanocrystalline Fe.[11] Therefore, surface and interface effects give nanostructured systems a two-phase character. Actually, two such phases do interact, giving rise to exchange anisotropy, as found in both oxide particles[8,12] and metallic systems.[10] Such surface and interface effects, which are strongly dependent on the particle size and its distribution, give an important contribution to the total particle anisotropy. Moreover, in the presence of interparticle interactions, the characteristics of the medium in which the particles are embedded and its ability to transmit exchange interactions have to be taken into account.[13,14]

In this framework, we have studied samples obtained by cold compaction of Fe nanoparticles surrounded by an oxide surface layer, prepared through the inert gas condensation (IGC) technique and oxygen passivation. Samples with different Fe to oxide weight fraction ratios (0.2–1.4) were synthesized by operating a control on the mean size of the metallic core, varying from 6 to 15 nm. The compositional, structural, and magnetic properties were investigated by means of transmission electron microscopy, x-ray diffraction, Mössbauer spectroscopy, and magnetization measurements in the 5–300-K temperature range. The obtained results provide a clear picture of the dependence of the magnetic properties on the Fe particle mean size and on the Fe and oxide fractions, throwing light on some aspects of the low-temperature dynamical magnetic behavior that to our knowledge were not addressed in a systematic way in previous investigations on similar systems.[15–21]

The magnetic behavior of the system has been found to be strongly dependent on the exchange coupling between the metallic crystallites, with a spin-ordered configuration, and the disordered (both structurally and magnetically) oxide phase. Such an exchange coupling gives rise to a frozen disordered state of the system at low temperatures and determines the temperature variation of the magnetic properties.

II. EXPERIMENT

Fe nanoparticles were produced by the IGC method:[22] 99.98% purity Fe was evaporated in a tungsten boat located in a chamber filled with He at a pressure of 133 Pa. Aerosol iron nanoparticles accumulated on a metallic rotating drum cooled by liquid N_2; then they were exposed to a mixture of 133-Pa O_2 and 1200-Pa He for 12 h to achieve passivation. Transmission electron microscopy (TEM) observations were performed on nanoparticles collected on a carbon-coated copper grid put inside the evaporation chamber during the synthesis process. A microscope Philips Tecnai *F*30, equipped with a Gif 2 K×2 K CCD camera, was used.

Nanoparticles with an increasing mean size have been obtained by increasing the current crossing the tungsten boat, and hence the vapor temperature, during three evaporation processes. After the passivation, the particles were scraped from the cold finger and pressed in high vacuum with a uniaxial pressure of 1.5 GPa, to obtain the pellets labeled *D*6, *D*10 and *D*15.

The pellets were investigated by x-ray diffraction (XRD) using a Philips PW1710 diffractometer with Cu$K\alpha$ radiation. Samples of magnetic characterization were obtained by the subsequent fragmentation of the compacted pellets in a powder of micrometric size. Each micrometric fragment consisted of a dense agglomerate of nanoparticles. Low-temperature magnetic properties of the samples have been investigated by means of a commercial superconducting quantum interference device magnetometer operating in the range 5–300 K and equipped with a superconducting magnet (H_{max}=55 kOe) and a special software option allowing us to fully control the warming/cooling rates (e.g., 4 K/min for the present experiments).

III. RESULTS

A. Structural properties

1. Transmission electron microscopy

Figure 1(a) shows the TEM micrograph of a typical Fe particle obtained by IGC and oxygen passivation. The dark core corresponds to metallic iron whereas the surrounding light gray layer is the oxide phase. The thickness of such layer is ~2 nm, independently on the Fe core size. The TEM contrast of the oxide phase resembles that of an amorphous structure and the presence of crystallites in this small region is hardly detectable [Figs. 1(b) and 1(c)]. The interface region between metallic core and oxide phase appears as a rather sharp boundary due to Fresnel fringes [Fig. 1(c)].

The TEM analysis reveals that the as-prepared particles are not always distinguishable as singular and well-separated entities, as shown in Fig. 1(a). More generally, the products of the evaporation and passivation procedures are agglomerates of several nanoparticles.

As shown in Fig. 1(d) in the case of small Fe cores (mean diameter <10 nm), these are well separated by the oxide even if small contact regions may exist. Larger metallic cores exhibit an enhanced tendency to merge together forming welded-neck junctions and grain boundaries [Fig. 1(e)]. Moreover, it has been generally noted that the metallic cores

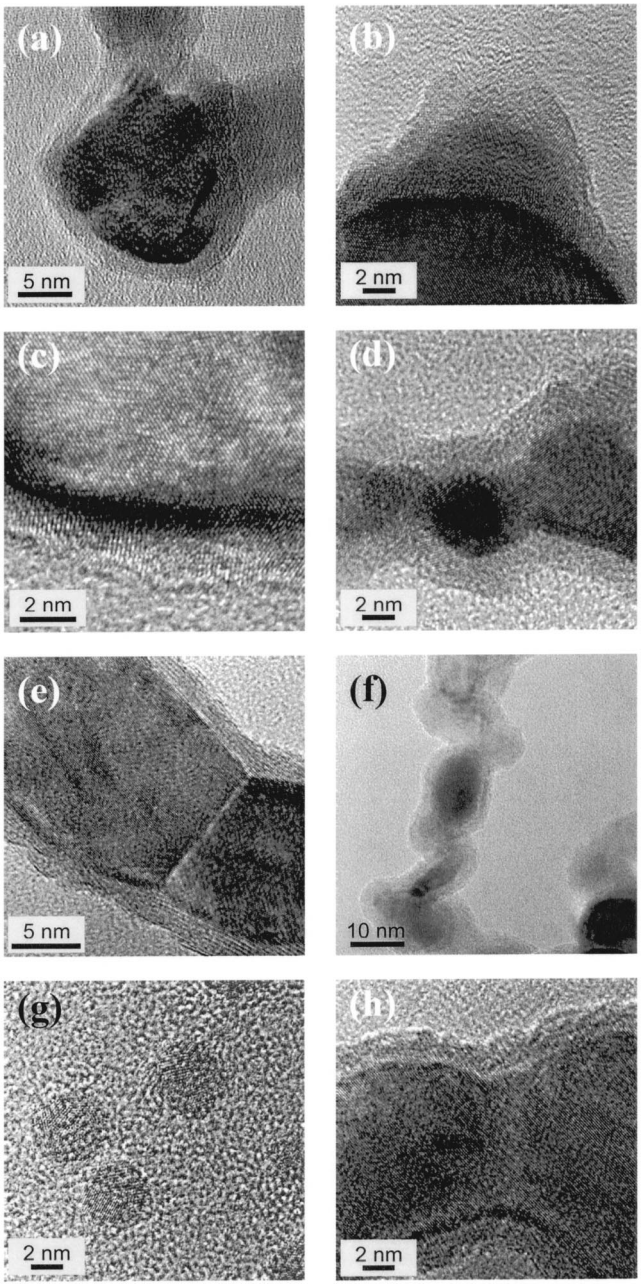

FIG. 1. TEM micrographs of oxygen passivated Fe nanoparticles produced by IGC. See the text.

have an elongated shape [Fig. 1(f)], characteristic that increases with increasing the Fe core dimensions. As a matter of fact, we have found that very fine particles, with a mean size below 5 nm, present a spherical shape, as shown in Fig. 1(g). Note that such particles do not show the characteristic core-shell morphology because they are so small that the passivation procedure induced their complete oxidation (each one consists of several crystal grains). In agreement with previous studies,[23] our findings seem to indicate that during a synthesis process carried out at low vapor temperature, the growth of small spherical particles, similar to those shown in Fig. 1(g), occurs by aggregation of atoms. At a high vapor temperature, the coalescence of the primary particles seems to be particularly favored: larger Fe cores are

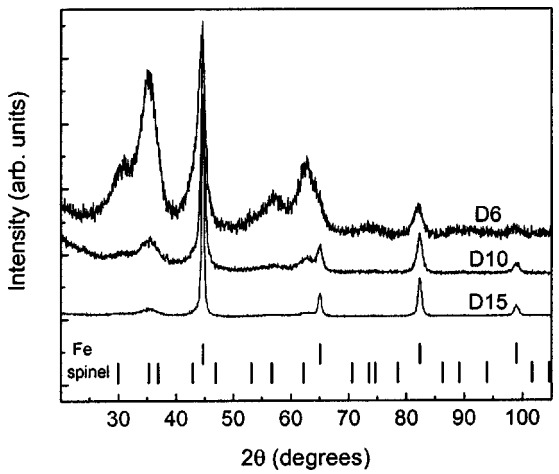

FIG. 2. XRD spectra for samples $D6$, $D10$, and $D15$.

obtained whose symmetry departs more and more from the spherical one [Fig. 1(h) shows the detail of the incomplete coalescence of two metallic cores].

2. X-ray diffraction

The XRD spectra of the samples $D6$, $D10$, and $D15$ are shown in Fig. 2. Two components are detected: the peaks of bcc Fe and the broadened and overlapping peaks of the oxide phase. The position and the integrated intensity of the latter correspond to the values usually quoted for magnetic (Fe_3O_4) and maghemite (γ-Fe_2O_3), both having spinel structure. However, the peak broadening does not allow us to distinguish between them. No reflection different from those of the cubic spinel structure has been observed.

XRD patterns was analyzed using a full profile-fitting program[24] following the Rietveld method [25] and assuming a spinel structure for the oxide phase. In particular, the refinement of the peak profile parameters and the quantitative phase analysis of the program have been used to determine the volume averaged grain size (D), the microstrain ($\langle \varepsilon^2 \rangle^{1/2}$) of the iron and oxide phases, and their volume (and weight) fractions. Such an analysis was carried out on a series of more than 20 samples including $D6$, $D10$, and $D15$.[26]

For both phases the intensity and width of the peaks are consistent with an isotropic model for crystallite size and strain. The results obtained for the Fe component are summarized in Table I. The Fe fraction increases with increasing D. Due to the particular morphology of the compacted nanoparticles, namely, the characteristic core-shell structure evidenced by TEM (Fig. 1), we consider that the volume averaged grain size D provides a measure of the mean size of the Fe cores. We recall that, for any distribution of spherical particles, D is related to the volume weighted diameter d by $D=\frac{3}{4}\ d$.[27] For nonspherical particles distributed in shape, a different proportionality constant is expected, which cannot be derived analytically. Also in this last case, valuable information can be obtained by assuming a log-normal distribution of spherical particles with respect to the diameter d.[28] The width of the distribution $\log \sigma$ can be expressed by mean of the ratio of the volume-weighted and area-weighted grain size D.[27] We have found that $\log \sigma$ varies between 0.41 and 0.49, and it is not correlated to the mean diameter. Such values are in agreement with those typically reported for a size distribution of gas-evaporated nanoparticles.[28] In the series of 20 samples, the observed trend of the iron volume fraction vs D was also in agreement with the assumption of spherical core-shell particles with a shell thickness of $\sim$2.5 nm, independent on the particle size, distributed according to a log-normal distribution with width $\log \sigma = 0.46$ (this last value was determined from the average over the 20 samples).[26]

For the oxide lattice parameter, the Rietveld analysis provides an intermediate value between those of magnetite and maghemite (8.399–8.335 Å). Indeed, we cannot exclude that the oxide phase is a mixture of both Fe_3O_4 and γ-Fe_2O_3, as suggested in various research works on similar samples.[16,17] The average grain size of the oxide phase is $\sim$2 nm and the microstrain is about one order of magnitude larger than for the metallic phase. The very small grain size and the high value of microstrain suggest that the oxide is a defective spinel due to the high structural and topological disorder. A cation disorder (i.e., a nonzero occupation factor of the octahedral c sites of the spinel structure and a reduction of the occupation factor for the usually occupied octahedral d sites) has been assumed to account for the (small) increase in the integrated intensity of the (440), with respect to polycrystalline magnetite or maghemite.

B. Magnetic properties

1. Magnetization vs field measurements

Hysteresis loops were measured on samples $D6$, $D10$, and $D15$ at different temperatures T between 5 and 300 K. The loops at $T=5$ K are displayed in Fig. 3. The values of magnetization $M_{(5T\text{-}5\,\mathrm{K})}$ at $H=50$ kOe and $T=5$ K are reported in Table II together with the extrapolated (at $1/H$ tending to

TABLE I. Results of the Rietveld analysis on the XRD spectra in Fig. 2. D and $\langle \varepsilon^2 \rangle^{1/2}$ are the volume averaged grain size and the microstrain of the Fe phase, respectively. The Fe fraction (volume and weight) and the oxide fraction (weight) are also reported.

Sample	D (nm) ($\pm$10%)	$\langle \varepsilon^2 \rangle^{1/2}$ (10^{-3}) ($\pm$10%)	Fe volume (%) ($\pm$3)	Fe weight (%) ($\pm$3)	Oxide weight (%) ($\pm$3)
$D6$	5.6	14	13	18	82
$D10$	9.6	9	21	28	72
$D15$	15.2	3	48	59	41

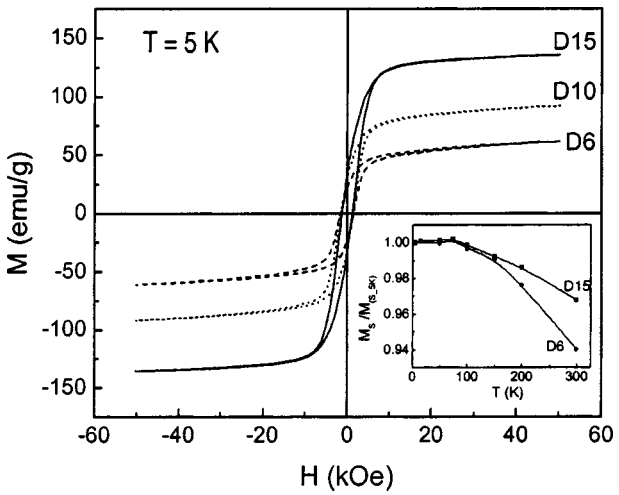

FIG. 3. Hysteresis loops measured at $T=5$ K on samples $D6$, $D10$, and $D15$. Inset: M_S vs T for samples $D6$ and $D15$ (normalized to the M_S value at $T=5$ K, $M_{S\_5\,\mathrm{K}}$)

zero) saturation values ($M_{(S\text{-}5\,\mathrm{K})}$). They increase with increasing D and with the Fe content. Such values are compared to those calculated (M_{calc}) considering the amounts of Fe and oxide derived from the XRD analysis (for the oxide phase we have considered a magnetization of 86 emu/g, corresponding to the average of bulk Fe_3O_4 and γ-Fe_2O_3). The ratio between $M_{(S\_5\,\mathrm{K})}$ and M_{calc} is also reported in Table II. The smaller D is, the lower the $M_{(S\_5\,\mathrm{K})}/M_{\mathrm{calc}}$ ratio.

In the inset of Fig. 3, for $D6$ and $D15$, the M_S values, normalized to $M_{(S\_5\,\mathrm{K})}$, are reported as a function of temperature. The curves are not fitted by a $T^{3/2}$ law.

The coercivity H_C is reported as a function of temperature in Fig. 4(a): H_C decreases with temperature for the three samples, the variation being more marked with decreasing D. In fact, at $T=5$ K, H_C decreases with increasing D, whereas at $T=300$ K it increases with D.

The loops in Fig. 3 show a nonsaturating character and a high value of the irreversibility field (H_{irr}). This is defined as the field above which the two branches of the loop in the first quadrant merge together in a single curve, the two corresponding magnetization values differing for less than 1%. At $T=5$ K, H_{irr} has the largest value for $D6$ ($\sim$28 kOe), and it decreases with increasing D [Fig. 4(b)]; in $D6$ it decreases with temperature up to $\sim$100 K and then it remains almost constant above $\sim$150 K. As for H_C, a weaker thermal dependence is observed in $D10$ and still weaker in $D15$. The

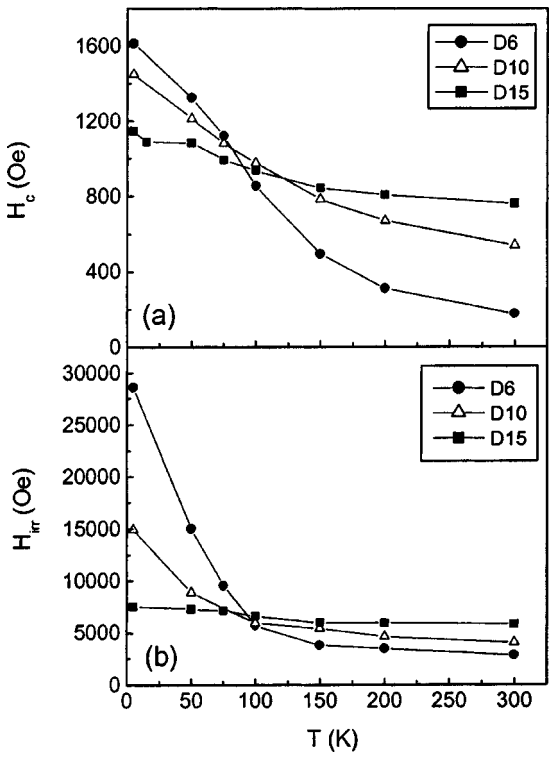

FIG. 4. Coercivity H_C (a) and irreversibility field H_{irr} (b) as functions of temperature for samples $D6$, $D10$, and $D15$.

non-saturating tendency, well noticeable in $D6$, increases with reducing temperature, especially below $\sim$50 K. This effect can be visualized by plotting the value of the slope (dM/dH) of the virgin magnetization curves in the field range 20–50 kOe, as a function of temperature (Fig. 5).

For sample $D6$, the virgin curves at $T=5$ and 300 K are shown in Fig. 6: at 5 K the curve is S shaped (this characteristic becomes more pronounced with decreasing D) whereas at 300 K it has an almost continuous downward curvature. The field derivative dM/dH of the virgin curves shows a peak at H^* (inflection field): H^* increases with decreasing temperature, the increase being more marked below $T\sim150$ K (inset of Fig. 6).

Hysteresis loops were measured after cooling the sample in a magnetic field of 20 kOe, from $T=300$ K down to a fixed temperature. At $T=5$ K, a shift of the loop towards the negative field has been observed for the three samples. The amount of the shift is usually quantified through the positive exchange field parameter $H_{\mathrm{ex}}=-(H_{\mathrm{right}}+H_{\mathrm{left}})/2$, where the

TABLE II. $M_{(5T\_5\,\mathrm{K})}$, magnetization measured at $T=5$ K and at $H=50$ kOe; $M_{(S\text{-}5\,\mathrm{K})}$, $1/H$ extrapolation of the magnetization at $T=5$ K; M_{calc} is the calculated magnetization starting from a XRD estimation of the constituent phases in Table I.

	$M_{(5T\_5\,\mathrm{K})}$ (emu/g) (±0.5)	$M_{(S\_5\,\mathrm{K})}$ (emu/g) (±0.5)	M_{calc} (emu/g) (±9)	$M_{(S\_5\,\mathrm{K})}/M_{\mathrm{calc}}$ (%) (±5)
$D6$	61.4	68.8	110	62
$D10$	89.7	95.9	123	78
$D15$	135.8	141.2	165	86

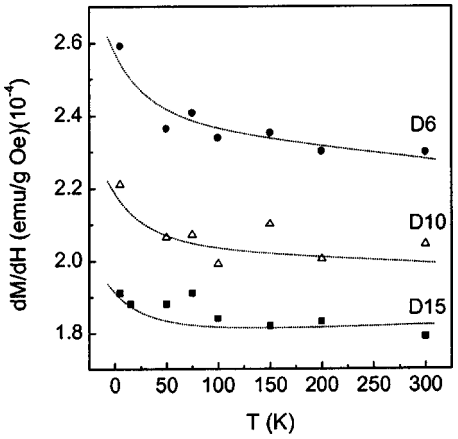

FIG. 5. Slope (dM/dH) of the virgin magnetization curves in the field range 20–50 kOe as a function of temperature, for samples $D6$, $D10$, and $D15$. The dotted lines are guides for the eye.

meaning of $H_{\rm right}$ and $H_{\rm left}$ is obvious. In Fig. 7, $H_{\rm ex}$ has been reported as a function of temperature for the three samples. $H_{\rm ex}$ increases with decreasing D; for all the samples, it decreases with temperature and it vanishes at $T\sim 150$ K.

2. Zero-field-cooled and field-cooled magnetizations

Magnetization measurements as a function of temperature were performed according to the zero-field-cooling (ZFC)—field-cooling (FC) procedure at different applied magnetic field ($10\ {\rm Oe}\leqslant H_{\rm appl}\leqslant 20$ kOe). $M_{\rm ZFC}$ was measured on warming from 5 to 300 K whereas $M_{\rm FC}$ was recorded during the subsequent cooling. Figure 8 shows the main results for sample $D6$. For measurements at $H_{\rm appl}<1000$ Oe, an irreversible magnetic behavior (difference between $M_{\rm FC}$ and $M_{\rm ZFC}$) is observed in the whole temperature range. We define the irreversibility temperature ($T_{\rm irr}$) as the temperature where the difference between $M_{\rm FC}$ and $M_{\rm ZFC}$, normalized to its maximum value at $T=5$ K, becomes smaller than 3%. On increasing $H_{\rm appl}$ from 1000 to 20 kOe (Fig. 8), $T_{\rm irr}$ reduces

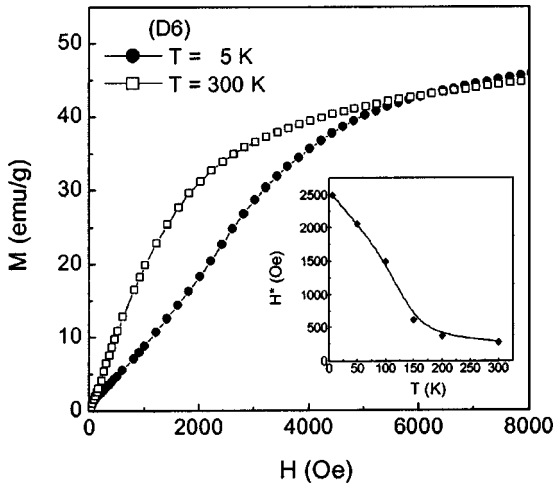

FIG. 6. Initial magnetization curves as a function of magnetic field at $T=5$ K, and 300 K for sample $D6$. Inset: inflection field (H^*) as a function of temperature for sample $D6$.

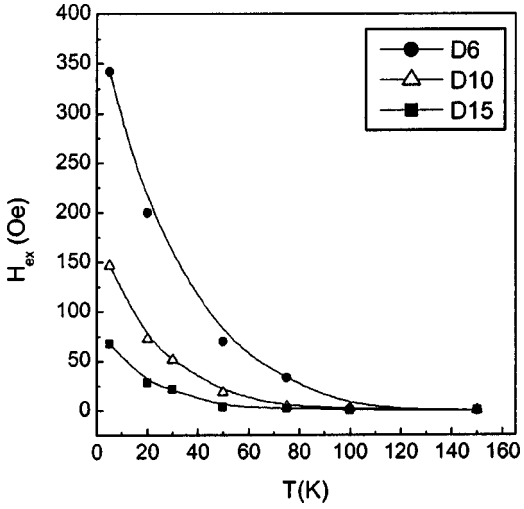

FIG. 7. Exchange field ($H_{\rm ex}$) as a function of temperature for samples $D6$, $D10$, and $D15$.

but the magnetic irreversibility persists at low temperature even under the largest $H_{\rm appl}$. In fact, on lowering the temperature, $M_{\rm FC}$ shows a very weak variation whereas $M_{\rm ZFC}$ starts to decrease below $T_{\rm irr}$.

The temperature derivative of the difference ($M_{\rm FC}-M_{\rm ZFC}$) has been calculated: some representative $[-d(M_{\rm FC}-M_{\rm ZFC})/dT]$ curves are shown in Fig. 9(a). For

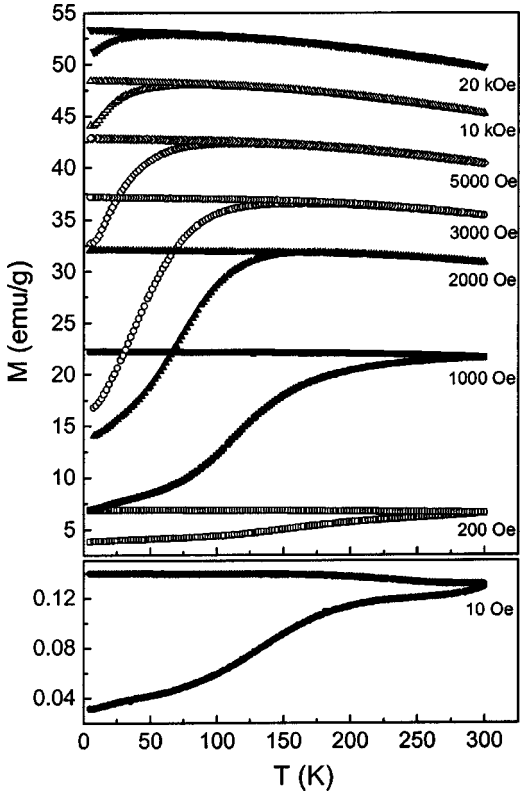

FIG. 8. Zero-field-cooling (ZFC, lower branch of each displayed curve) and field-cooling (FC, upper branch) magnetizations (M) as a function of temperature measured on sample $D6$ for different applied magnetic fields.

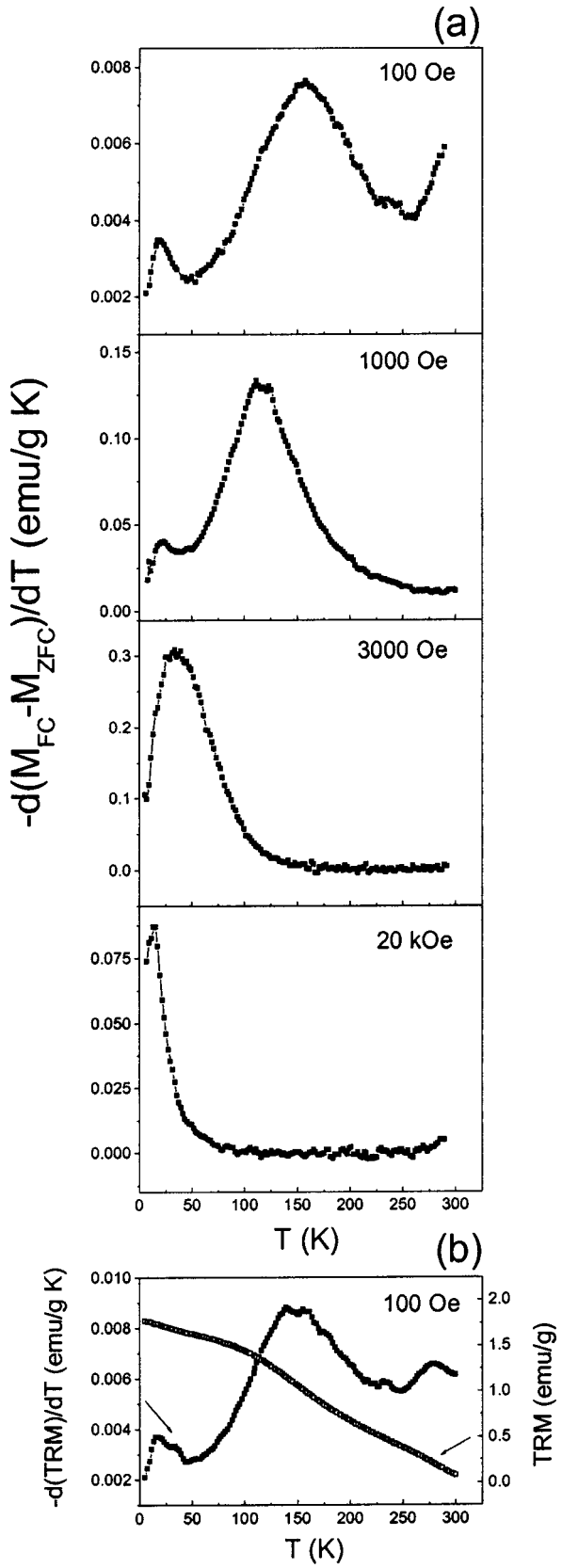

FIG. 9. (a) Temperature derivative $[-d(M_{\mathrm{FC}}-M_{\mathrm{ZFC}})/dT]$ of the difference between field-cooled and zero-field-cooled magnetizations measured on sample $D6$ at the indicated magnetic field. (b) Thermoremnant magnetization (TRM) measured on $D6$ at $H_{\mathrm{appl}}=100$ Oe and temperature derivative $[-d(\mathrm{TRM})/dT]$.

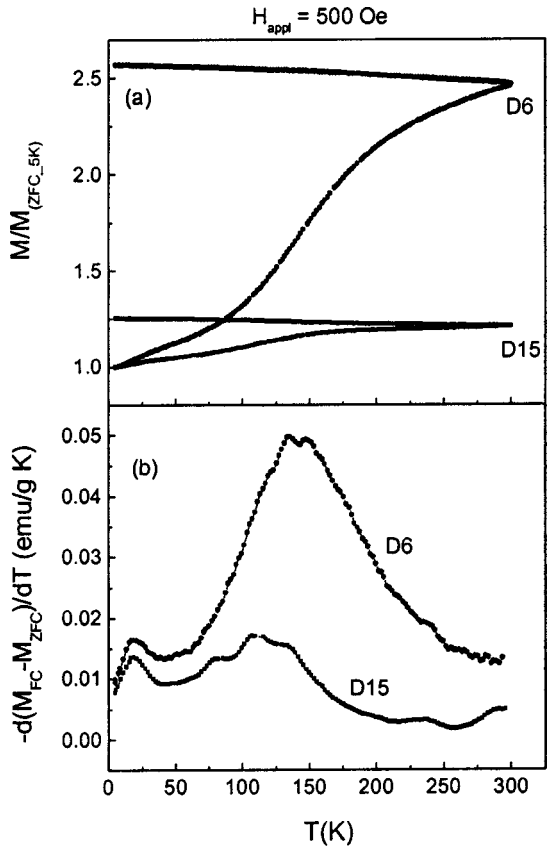

FIG. 10. (a) $M_{\mathrm{ZFC/FC}}$ as a function of temperature measured at $H_{\mathrm{appl}}=500$ Oe on samples $D6$ and $D15$. The curves are normalized to the value of M_{ZFC} at $T=5$ K ($M_{\mathrm{ZFC\_5\,K}}$). (b) Temperature derivative of the difference between field-cooled and zero-field-cooled magnetization shown in (a).

H_{appl} up to 200 Oe, they are characterized by the presence of two peaks—a small one at low temperature (peak temperature $T_1\sim 20$ K at $H_{\mathrm{appl}}=100$ Oe) and a larger one at higher temperature (peak temperature $T_2\sim 150$ K at $H_{\mathrm{appl}}=100$ Oe); a rising tendency starting from approximately 250 K. For higher fields, this last effect is no more visible; the larger peak, strongly field dependent, shifts to lower temperatures, toward the smaller one, exhibiting a weak field-dependence, and for $H_{\mathrm{appl}}=3000$ Oe they definitively merge. The low temperature peak is still visible at $H_{\mathrm{appl}}=20$ kOe.

A similar analysis was repeated on sample $D15$. In Fig. 10 we report (a) $M_{\mathrm{ZFC/FC}}$ vs T for $D6$ and $D15$ at $H_{\mathrm{appl}}=500$ Oe, normalized to the M_{ZFC} value measured at $T=5$ K ($M_{\mathrm{ZFC\_5\,K}}$), and (b) the corresponding $[-d(M_{\mathrm{FC}}-M_{\mathrm{ZFC}})/dT]$ curves. In these last curves, two peaks are well visible in both samples, but unlike the smaller peak—positioned at approximately the same temperature—the large one is shifted toward lower temperatures for $D15$ ($T_2\sim 110$ K).

IV. DISCUSSION

According to TEM images (Fig. 1) and considering the high oxide fraction (Table I), the material can be modeled in

terms of an iron oxide matrix in which nanometric Fe particles are dispersed. The oxide matrix is not a continuous medium: as the samples are obtained by the cold compaction of the as-prepared aggregates of core-shell nanoparticles [Figs. 1(d)–1(f)], a high fraction of pores is certainly present.[18] The oxide matrix is poorly crystallized [Figs. 1(b), 1(c), and 2].

Let us first discuss the properties of sample $D6$, in particular the hysteresis loop measured at $T=5$ K (Fig. 3). The large high-field slope (Fig. 5) and the small magnetization value at $H=50$ kOe, well below the expected one on the basis of the Fe and oxide weight fractions obtained by XRD (Table II), reveal a noncollinear arrangement of atomic spins. Similar effects were observed in nominally ferrimagnetic particles ($NiFe_2O_4$, γ-Fe_2O_3) and associated with a random spin canting at the outer particle layers.[7,29] Reduced coordination and hence broken superexchange bonds between surface spins result in an alteration of the orientation of each magnetic moment and hence in a disordered spin configuration and a reduction of the net average moment. Spin canting was also observed by Mössbauer spectroscopy in thin oxide layers on metallic Fe cores prepared by an aerosol method.[15] For our samples, a disordered spin configuration is expected to result from the intrinsic structural disorder of the oxide matrix in which the Fe particles are embedded.

Thermal fluctuations of canted surface spins in ferrimagnetic particles[7–9] as well as boundary spins in antiferromagnetic ball-milled FeRh (Ref. 10) and pure nanocrystalline Fe (Ref. 11) have been found to freeze at low temperature into a spin-glass-like phase with a multidegenerate ground state. The origin of this behavior was ascribed to the combination of structural disorder and frustration due to competing magnetic interactions. In our samples too, the spins of the structurally disordered oxide matrix could be frozen in a spin-glass-like state at low temperature. Such a picture is supported by the observed high-field irreversibility at low-temperature (e.g. for sample $D6$, $H_{irr}\sim 28$ kOe at $T=5$ K [Fig. 4(b)]). Hence, the shift of the field-cooled hysteresis loop at $T=5$ K (Fig. 7), can be associated with the exchange anisotropy originating from the exchange coupling between the spin-glass-like matrix and the ferromagnetic crystallites. At low temperature, the whole system should be in a disordered magnetic state, where the orientation of the oxide and Fe particle moments is affected by both particle-particle dipolar interactions and exchange coupling between the spin-glass-like matrix and the ferromagnetic phase.

The spin-glass-like state does not evolve in a pure paramagnetic or superparamagnetic regime with increasing temperature up to 300 K. In Fig. 8, for $H_{appl}<1000$ Oe, magnetic irreversibility persists for temperatures close to 300 K; with increasing H_{appl}, the shape of the M_{ZFC} curves exhibits a strong field dependence, suggesting blocking/freezing phenomena at field-dependent temperatures, with a ferromagneticlike trend of $M_{ZFC/FC}$ above T_{irr}. The Mössbauer analysis of the samples with different D (Ref. 26) indicates that, at $T=4.2$ K, the spectra can be well fitted using the characteristic six-line pattern of bcc Fe, given by the metallic particles, plus two wide sextets for the oxide component, consistent with structural disorder. The Fe and oxide volume

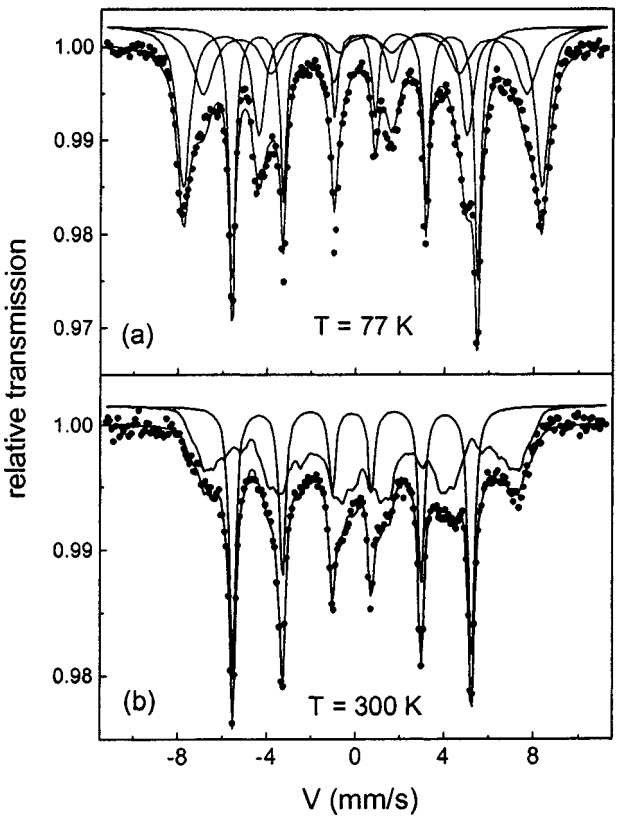

FIG. 11. Mössbauer spectra at $T=77$ K (a) and $T=300$ K (b) measured on an Fe/Fe oxide sample with structural features similar to $D10$.

fractions deduced from the resonant areas of the sextets are consistent, within 3%, with those obtained by XRD. No significant paramagnetic component is observed in the Mössbauer spectra up to room temperature. At $T=300$ K, the two oxide sextets are replaced by a broad relaxing component, superimposed to the bcc-Fe sextet. Typical Mössbauer spectra at $T=77$ (a) and 300 K (b) are shown in Fig. 11. Such a behavior was also observed by other authors on similar samples.[15,17]

Let us now consider the $[-d(M_{FC}-M_{ZFC})/dT]$ curves [Fig. 9(a)]. It is worth recalling that, in the presence of independent relaxation phenomena (i.e., noninteracting particles), the temperature derivative of the remnant magnetization reflects the effective distribution of anisotropy energy barriers of the system.[30] We found that such curve has the same trend as the temperature derivative of the difference between M_{FC} and M_{ZFC}, as shown in Fig. 9(b), where the thermoremnant magnetization (TRM) at $H_{appl}=100$ Oe and its temperature derivative are reported (the sample was cooled down from $T=300$ to 5 K in H_{appl}; then the field was removed and the remanence was measured for increasing T). Therefore, although in the present case the relaxation processes cannot be considered independent, qualitative information can be drawn from the analysis of the $[-d(M_{FC}-M_{ZFC})/dT]$ curves.

Common feature of all these curves is the presence of a well-defined peak at $T_1\sim 20$ K, which does not depend significantly on the magnetic field. This is consistent with the

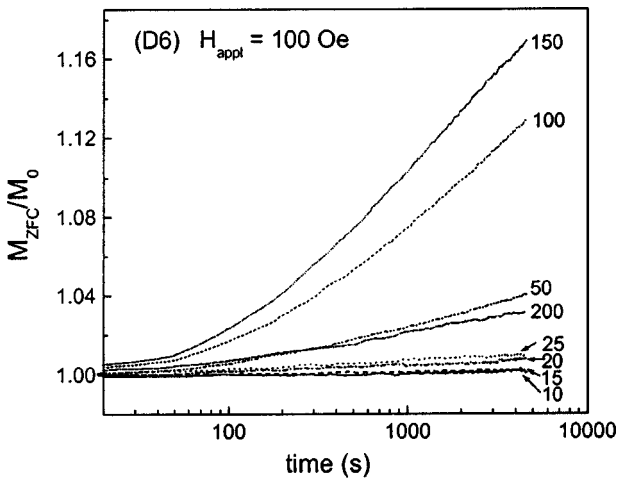

FIG. 12. M_{ZFC} as a function of time measured on sample $D6$ for $H_{appl}=100$ Oe at the indicated temperatures. M_0 is the magnetization at the beginning of the measurements.

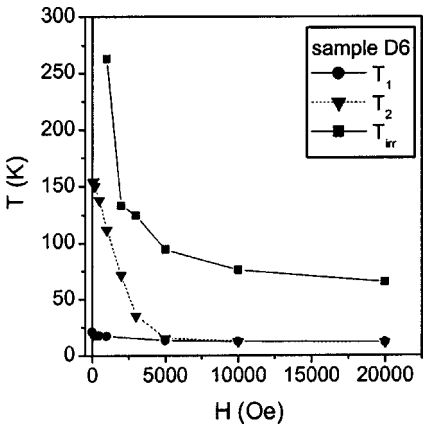

FIG. 13. Dependence of T_1, T_2, and T_{irr} on the applied magnetic field for sample $D6$.

hypothesized picture of a frozen, disordered magnetic state at low temperature: this is also confirmed by the lack of magnetic relaxation below $T=25$ K—as shown in Fig. 12, where the time dependence of M_{ZFC} is reported for sample $D6$ at different temperatures ($H_{appl}=100$ Oe; note that the maximum relaxation is measured at $T=150$ K).

Above T_1, a large peak is observed in the $[-d(M_{FC}-M_{ZFC})/dT]$ curve at low applied field ($H_{appl}\leqslant 100$ Oe) [Fig. 9(a)]. It becomes narrower and shifts to lower temperature with increasing field. This indicates the existence of a very broad, field-dependent energy barrier distribution. This is consistent with the existence of irreversibility well above T_1, and with the field dependence of the amplitude of $(M_{FC}-M_{ZFC})$ and of T_{irr} which decreases with increasing H above 1000 Oe (Fig. 8). T_{irr} signals the onset of a freezing process with decreasing temperature, i.e., the blocking associated to the highest anisotropy energy barrier. The dynamics slows down with decreasing temperature and at T_1 the whole system appears static on the experimental time scale.

On this basis, we can conveniently describe our system as constituted by two different components, strongly coupled at the interface: a nonrelaxing (quasistatic) ferromagnetic component and a relaxing, magnetically disordered component. The Fe particles provide the first component, whereas regions of exchange-interacting spins of the oxide matrix represent the second one.

Below T_1, the oxide region moments do not relax and are frozen in the spin-glass-like (or *cluster-glass-like*) state. On increasing the temperature above T_1, such a completely frozen state evolves into a regime where the oxide magnetic regions become progressively unfrozen, according to the distribution of effective anisotropy energy barriers, determined by their size and by the strength of the magnetic interaction with the surrounding. The large peak in the $[-d(M_{FC}-M_{ZFC})/dT]$ curve at low H_{appl} [Fig. 9(a)] reflects the width of such distribution. Once the net moments of the oxide magnetic regions become able to thermally fluctuate, they tend to be polarized by the Fe particle moments, which thus prevent (or shift to higher temperature) the passage into the superparamagnetic regime. This effect is boosted by the magnetic field, which favors the formation of a *ferromagnetic network* throughout the sample. We can assume that the polarizing, ferromagnetic component gives rise to an increasing background in the zero-field-cooled susceptibility vs temperature curve, coherently with the rising tendency in M_{ZFC} (and hence in $[-d(M_{FC}-M_{ZFC})/dT]$) visible for $H_{appl}\leqslant 200$ Oe, starting from $T\sim 250$ K [Figs. 8 and 9(a)]. Similarly, the behavior of $[-d(\mathrm{TRM})/dT]$ above $T\sim 250$ K [Fig. 9(b)] can be ascribed to the presence of a background component associated to the nonrelaxing Fe particles.

The field dependences of T_1, T_2 and T_{irr} are reported in Fig. 13 for $D6$. The low-temperature region, delimited by the T_1 curve, corresponds to the completely frozen state. The region between T_1 and T_{irr} curves defines a regime consisting of frozen and relaxing oxide magnetic regions, which coexist with the quasistatic Fe component. Finally, above T_{irr}, all the oxide magnetic regions are unfrozen and polarized by the Fe particle moments. Note that we cannot define T_{irr} for $H_{appl}<1000$ Oe since M_{ZFC} and M_{FC} are forced to merge at the maximum measuring temperature of 300 K (Fig. 8).

With increasing T above 300 K, it is to be expected that the thermal fluctuations of the oxide moments, revealed by the room-temperature Mössbauer spectra analysis [Fig. 11(b)], become more and more rapid and that a temperature exists at which they finally enter the superparamagnetic regime, irrespective of the presence of the Fe particles and of the magnitude of H_{appl} (furthermore, some structural changes could occur in the samples upon annealing above room temperature.[31,18]) The Mössbauer spectrum in Fig. 11(b), showing the presence of a relaxing component, unambiguously indicates that such temperature must be much lower than the ordering temperature of both Fe_3O_4 (860 K) and γ-Fe_2O_3 (1020 K).

In other words, it can be assumed that the oxide matrix is characterized by a random magnetic anisotropy (locally varying easy axis and distribution of local anisotropy constant) that increases with decreasing temperature. At high temperature, where the oxide anisotropy is lower, the polarizing action of the Fe particle moments on the matrix moments dominates, and this implies an enhancement of the

degree of collinearity of the moments, as suggested by the reduced slope in the high-field region of the virgin magnetization curves (Fig. 5). With reducing temperature, the progressive freezing of the net moments of the oxide magnetic regions occurs along random anisotropy directions, giving rise to the increase of the high-field slope of the M vs H curves (Fig. 5). Accordingly, in $D6$ the initial M vs H curve is ferromagneticlike at $T=300$ K whereas at $T=5$ K it resembles that of frustrated systems like spin glasses (Fig. 6).[32]

A necessary condition for the observation of exchange bias is that the antiferromagnetic phase (or ferrimagnetic or spin glass) has a large magnetic anisotropy, so that it can exert a pinning action on the ferromagnetic phase. Basically, H_{ex} is expected to be proportional to the square root of the anisotropy constant of the antiferromagnetic phase.[33,8] In $D6$, H_{ex} appears below $T=150$ K (Fig. 7), i.e., in correspondence with the freezing of most of the moments of the oxide magnetic regions, as indicated by the position at about the same temperature of the large central peak in the $[-d(M_{FC}-M_{ZFC})/dT]$ curve at low H_{appl} [Fig. 9(a)]. With reducing temperature, H_{ex} shows a marked increase because of the progressive increase of anisotropy and the consequent freezing of more and more oxide region moments. It is worth noting that both H_C [Fig. 4(a)] and the inflection field (inset of Fig. 6) strongly increase with reducing T starting from $T\sim150$ K, coherently with the above picture. The thermal evolution of H_C in sample $D6$ [Fig. 4(a)] is explained considering that at very low temperature the frozen oxide matrix exerts a strong pinning action on the Fe particle moments, particularly effective because of the small D and hence of the high surface to volume ratio. At $T=300$ K, the oxide matrix is polarized by the Fe particles. Its contribution to H_C can be neglected compared to that of the Fe particles.

It is now useful to compare with samples $D10$ and $D15$. The features of the hysteresis loops reflect the differences in the chemical composition. $M_{(S\text{-}5\,K)}$ increases with the Fe content and the difference between the calculated and measured magnetization decreases, confirming that the oxide phase is responsible for the magnetization reduction (Fig. 3 and Table II). The nonrelaxing component, and hence the ferromagnetic character, increases with D, as revealed by the weaker thermal dependence of M_S (inset of Fig. 3), by the decrease of magnetic irreversibility in the $M_{ZFC/FC}$ curves [Fig. 10(a)] and by the reduced non-saturating tendency in the M vs H curves (Fig. 5).

The observation that the low-temperature peak in the $[-d(M_{FC}-M_{ZFC})/dT]$ curves at $H_{appl}=500$ Oe appears at the same temperature for $D6$ and $D15$ and that the strong peak is centered at a lower temperature T_2 in $D15$ [Fig. 10(b)] confirms that none of the two is directly related to the relaxation of the individual Fe particles. If this were the case, the larger size of the Fe particles in $D15$ should imply higher anisotropy energy barriers and hence the peaks should be centered at higher temperature. Actually, the peaks are associated with freezing processes involving spins of the oxide matrix. The low T_2 of $D15$, compared to $D6$, may be explained considering that the larger nonrelaxing ferromagnetic component in $D15$ causes a mean magnetic field that reduces the height of the energy barriers of the relaxing component and shifting the energy barrier distribution to lower values.

H_C and H_{ex} at $T=5$ K increase with decreasing D [Figs. 4(a) and 7] revealing that exchange anisotropy effects at the interface between particles and matrix are more important when the surface to volume ratio of the particles increases. To gain insight into the exchange bias phenomenon, a useful starting point is the Meiklejohn-Bean model which predicts, for materials with ferromagnetic (FM)/antiferromagnetic (AFM) interfaces, the relation[34]

$$H_{ex}\cong J_{int}/M_{FM}t_{FM}, \tag{1}$$

where J_{int} is the exchange constant across the FM/AFM interface per unit area, and M_{FM} and t_{FM} are the magnetization and the thickness of the FM layer, respectively. It should be noted that important parameters are not considered in Eq. (1), such as the AFM layer anisotropy and thickness, the noncollinearity of the AFM-FM spins, and the formation of domains in the AFM and FM layers.[33] For real granular systems, the particle random orientation, the distribution of particle sizes and shapes, the difficulty to characterize the microstructure of the interface, and, in our case, the spin-glass-like nature of the oxide matrix make it difficult to extract quantitative information. Nevertheless, the observed increase of H_{ex} with decreasing D at $T=5$ K (Fig. 7) constitutes an interesting result, resembling the $1/t_{FM}$ dependence of Eq. (1). A necessary condition for the observation of exchange anisotropy is[34]

$$K_{AFM}t_{AFM}\geqslant J_{int}, \tag{2}$$

where K_{AFM} and t_{AFM} are the anisotropy and the thickness of the AFM layer, respectively.

In our case, if one assumes for M_{FM} the value of bulk Fe (1714 emu/cm^3), for t_{FM} the mean particle size D and for t_{AFM} the double of the oxide shell thickness ($\sim$4 nm), Eq. (1) yields $J_{int}=0.35$ ergs/cm^2 for sample $D6$ and then $K_{AFM}\geqslant 9\times10^5$ ergs/cm^3 from Eq. (2); for $D15$, $K_{AFM}\geqslant 4\times10^5$. Hence, K_{AFM}, namely, the oxide matrix anisotropy, must be at least one order of magnitude larger than the magnetocrystalline anisotropy of bulk γ-Fe_2O_3 (4.6×10^4 ergs/cm^3), and definitely larger than that of Fe_3O_4 (1×10^5 ergs/cm^3). Such estimation is in agreement with the value found in γ-Fe_2O_3 nanoparticles (7×10^5 ergs/cm^3) and associated with surface with finite-size effects.[8,35]

As observed for $D6$, in sample $D15$ H_{ex} appears below the temperature T_2 of the large central peak in the $[-d(M_{FC}-M_{ZFC})/dT]$ curve and then increases with reducing T. The temperature dependence of H_C, H_{irr}, and H_{ex} becomes weaker with increasing D due to the increase in the ferromagnetic character and to the reduced oxide fraction.

On samples obtained by compacting Fe nanoparticles produced by IGC and not subjected to passivation, Löffler *et al.* found, at $T=300$ K, and $H_C\sim30$ Oe for $D\sim10$ nm (the maximum $H_C\sim100$ Oe was measured for $D\sim30$ nm).[18] Their results have been explained considering that, despite the presence of voids and pores in the structure, the exchange interaction is able to couple the Fe particle moments, as described by the random anisotropy model for nanocrystalline materials. The high room-temperature values of H_C of our

samples rule out the possibility that the Fe particles are so exchange coupled and support the hypothesis that they are predominantly magnetic single domain. Hence, the oxide matrix does not transmit the exchange interaction to neighboring Fe particles: this indicates a low effective exchange stiffness constant of the oxide matrix, which is consistent with the relaxing behavior of the oxide moments, as revealed by the Mössbauer analysis [Fig. 11(b)].

At $T=300$ K, we could expect that an estimation of H_C is obtained by the Stoner-Wohlfarth model, according to which, for randomly oriented spherical single-domain Fe particles, the maximum coercivity value is given by the expression $H_C=0.64\ K_{\mathrm{Fe}}/M_S$, and amounts to $\sim$180 Oe ($K_{\mathrm{Fe}}=4.8\times10^5$ erg/cm^3, the magnetocrystalline anisotropy of bcc Fe).[36] H_C of $D6$ is in agreement with such a prediction, but in $D15$ $H_C\sim800$ Oe. This could be due to the presence of a shape anisotropy contribution to the total anisotropy, becoming more and more noticeable with increasing D, as confirmed by TEM analysis [Figs. 1(e), 1(f), and 1(h)].

V. CONCLUSIONS

The low-temperature magnetic properties of samples obtained by cold-compacting core-shell Fe/Fe oxide nanoparticles have been investigated, and their dependence on the structure, composition, and mean particle size D has been discussed. The compacted samples have been described in terms of a disordered oxide matrix in which the Fe particles are dispersed.

The magnetization results support a simplified picture of samples consisting of two different magnetic components: a ferromagnetic quasistatic component, corresponding to the Fe particle moments; and a relaxing one, represented by magnetically and structurally disordered oxide regions of exchange-interacting spins. The effective distribution of anisotropy energy barriers for the relaxing component is very broad and strongly field dependent.

At room temperature, most of the net moments of the oxide regions thermally fluctuate and tend to be polarized by the Fe particle moments. With decreasing temperature, a progressive freezing of the moments of the oxide matrix occurs at field-dependent temperatures, according to the distribution of anisotropy energy barriers. Finally, below a weakly field-dependent temperature T_1, the freezing of the oxide matrix in a spin-glass-like state is complete and the interplay between matrix-particle exchange coupling and particle-particle dipolar interactions results in a frozen disordered magnetic state for the whole system. Such description is supported by the lack of magnetic relaxation below $T\sim25$ K, the analysis of the $M_{\mathrm{ZFC/FC}}$ vs T curves and by the thermal dependence of the exchange field H_{ex} and coercivity H_C. With decreasing temperature from 300 K, H_{ex} strongly increases at a temperature at which most of the oxide region moments freeze, consistently with the derived anisotropy energy barrier distribution. Below the same temperature, H_C increases too.

Hence, with varying temperature, the magnetic coupling between Fe particles and the oxide matrix gives rise to various magnetic behaviors, the difference being essentially determined by the change in the oxide phase anisotropy. Below $T_1\sim20$ K, such an anisotropy is larger compared to bulk γ-Fe_2O_3 and Fe_3O_4, and the exchange bias effect between iron and oxide phases is maximized.

The comparison between samples with different mean particle size D (6, 10, and 15 nm) supports our description. In particular, the smaller magnetic irreversibility, the reduced nonsaturating tendency in the M vs H curves, the lower T_2, and the weaker temperature dependence of H_C in samples with larger D are all consistent with the presence of a larger static, ferromagnetic component. At $T=5$ K, the increase in H_C and H_{ex} with decreasing D reveals that the exchange coupling at the interface between particles and matrix is enhanced when the surface to volume ratio of the particles increases. At $T=300$ K, the high H_C value ($180\leqslant H_C<800$ Oe), with respect to compacted ferromagnetic nanoparticles,[18] indicates that the relaxing oxide matrix is not able to transmit the exchange interaction to neighboring Fe particles that are essentially single domain; the strong increase of H_C as D increases should be mainly due to the contribution of shape anisotropy, since with increasing D the symmetry of the particles deviates more and more from the spherical one, as indicated by TEM observations.

ACKNOWLEDGMENTS

This work was partially supported by the Istituto Nazionale per la Fisica della Materia (INFM) under Project No. PRA-ELTMAG. The authors are gratefully indebted to Dr. J. M. Grenèche (Université du Maine, France) for performing the Mössbauer measurements and for discussion. Dr. C. Beeli (ETH-Zurich, Switzerland) is acknowledged for a discussion on the electron microscopy results.

*Corresponding author. Email address: delbianco@df.unibo.it

[1] Y. Yoshizawa, S. Oguma, and K. Yamauchi, J. Appl. Phys. **64**, 6044 (1988).

[2] A. Manaf, M. Leonowicz, H. A. Davies, and R. A. Buckley, J. Appl. Phys. **70**, 6366 (1991).

[3] B. Dieny, V. S. Speriosu, S. S. P. Parkin, B. A. Gurney, D. R. Wilhoit, and D. Mauri, Phys. Rev. B **43**, 1297 (1991).

[4] P. Allia, M. Knobel, P. Tiberto, and F. Vinai, Phys. Rev. B **52**, 15 398 (1995).

[5] R. F. Ziolo, E. P. Giannelis, B. Weinstein, M. P. O'Horo, B. N. Ganguly, V. Mehrotra, M. W. Russell, and D. R. Huffman, Science **257**, 219 (1992).

[6] S. Y. Chou, P. R. Krauss, and L. Kong, J. Appl. Phys. **79**, 6101 (1996).

[7] R. H. Kodama, A. E. Berkowitz, E. J. McNiff, and S. Foner, Phys. Rev. Lett. **77**, 394 (1996).

[8] B. Martinez, X. Obradors, Ll. Balcells, A. Rouanet, and C. Monty, Phys. Rev. Lett. **80**, 181 (1998).

[9] E. Tronc, A. Ezzir, R. Cherkaoui, C. Chanéac, M. Noguès, H. Kachkachi, D. Fiorani, A. M. Testa, J. M. Grenèche, and J. P. Jolivet, J. Magn. Magn. Mater. **221**, 63 (2000).

[10] A. Hernando, E. Navarro, M. Multigner, A. R. Yavari, D. Fiorani,

M. Rosenberg, G. Filoti, and R. Caciuffo, Phys. Rev. B **58**, 5181 (1998).
[11] E. Bonetti, L. Del Bianco, D. Fiorani, D. Rinaldi, R. Caciuffo, and A. Hernando, Phys. Rev. Lett. **83**, 2829 (1999).
[12] R. H. Kodama, S. A. Makhlouf, and A. E. Berkowitz, Phys. Rev. Lett. **79**, 1393 (1997).
[13] T. Jonsonn, P. Svedlindh, and M. F. Hansen, Phys. Rev. Lett. **81**, 3976 (1998).
[14] D. Fiorani, J. L. Dormann, R. Cherkaoui, E. Tronc, F. Lucari, F. D'Orazio, L. Spinu, M. Nogues, A. Garcia, and A. M. Testa, J. Magn. Magn. Mater. **196–197**, 143 (1999).
[15] K. Haneda and A. H. Morrish, Surf. Sci. **77**, 584 (1978).
[16] K. Haneda and A. H. Morrish, Nature (London) **282**, 186 (1979).
[17] S. Gangopadhyay, G. C. Hadjipanayis, B. Dale, C. M. Sorensen, K. J. Klabunde, V. Papaefthymiou, and A. Kostikas, Phys. Rev. B **45**, 9778 (1992).
[18] J. F. Loffler, J. P. Meier, B. Doudin, J. P. Ansermet, and W. Wagner, Phys. Rev. B **57**, 2915 (1998).
[19] S. Gangopadhyay, G. C. Hadjipanayis, C. M. Sorensen, and K. J. Klabunde, J. Appl. Phys. **73**, 6964 (1993).
[20] H. Kisker, T. Gessmann, R. Würschum, H. Kronmüller, and H. E. Schaefer, Nanostruct. Mater. **6**, 925 (1995).
[21] L. Del Bianco, A. Hernando, M. Multigner, C. Prados, J. C. Sànchez-Lopez, A. Fernandez, C. F. Conde, and A. Conde, J. Appl. Phys. **84**, 2189 (1998).
[22] R. Birringer, H. Gleiter, H. P. Klein, and P. Marquardt, Phys. Lett. **102A**, 365 (1984).
[23] R. C. Flagan, in *Nanostructured Materials, Science & Technology*, NATO Advanced Study Institute Series, edited by G. M. Chow and N. I. Noskova (Kluver, Dordrecht, 1998), p. 15.
[24] L. Lutterotti and P. Scardi, J. Appl. Crystallogr. **23**, 246 (1990).
[25] H. M. Rietveld, Acta Crystallogr. **20**, 508 (1966).
[26] L. Savini, Ph.D. thesis, University of Bologna, 2002.
[27] J. I. Langford, D. Louër, and P. Scardi, J. Appl. Crystallogr. **33**, 964 (2000).
[28] C. G. Granqvist and R. A. Buhrman, J. Appl. Phys. **47**, 2200 (1976).
[29] J. M. D. Coey, Phys. Rev. Lett. **27**, 1140 (1971).
[30] K. O'Grady and R. W. Chantrell, in *Magnetic Properties of Fine Particles*, edited by J. L. Dormann and D. Fiorani (North-Holland, Amsterdam, 1992), p. 93.
[31] C. Prados, M. Multigner, A. Hernando, J. C. Sanchez, A. Fernandez, C. F. Conde, and A. Conde, J. Appl. Phys. **85**, 6118 (1999).
[32] P. Zhang, F. Zuo, F. K. Urban III, A. Khabari, P. Griffiths, and A. Hosseini-Tehrani, J. Magn. Magn. Mater. **225**, 337 (2001).
[33] Review: J. Nogués and I. K. Schuller, J. Magn. Magn. Mater. **192**, 203 (1999).
[34] W. H. Meiklejohn, J. Appl. Phys. **33**, 1328 (1962).
[35] B. Martinez, A. Roig, X. Obradors, E. Molins, A. Rouanet, and C. Monty, J. Appl. Phys. **79**, 2580 (1996).
[36] E. C. Stoner and E. P. Wohlfarth, Proc. Phys. Soc., London, Sect. A **240**, 599 (1948).